Dynamics of droplet consumption in Vapor-Liquid-Solid III-V nanowire growth

Anton Pishchagin, Frank Glas, Gilles Patriarche, Andrea Cattoni, Jean-Christophe Harmand, Fabrice Oehler

Dynamics of droplet consumption in vapor-liquid-solid III-V nanowire growth

Anton Pishchagin,*,† Frank Glas,*,† Gilles Patriarche,† Andrea Cattoni,†,‡ Jean-Christophe Harmand,† and Fabrice Oehler†

†*Université Paris-Saclay, CNRS, Centre de Nanosciences et de Nanotechnologies, 91120 Palaiseau, France*

‡*Institut Photovoltaïque d'Ile-de-France, 91120 Palaiseau, France*

E-mail: anton.pishchagin@c2n.upsaclay.fr; frank.glas@c2n.upsaclay.fr

Abstract

We study experimentally and theoretically the consumption of the apical gallium droplet that mediates the self-catalyzed vapor-liquid-solid growth of GaP nanowires. Consumption is achieved after growth by providing only phosphorous and its progress is monitored *ex situ* in nanowire arrays fabricated by molecular beam epitaxy. We develop detailed calculations of the process, taking into account four channels of liquid gallium consumption. These include the formation of GaP using phosphorous delivered to the droplet by direct impingement or after re-emission from the substrate. We show that two other channels contribute significantly, namely the diffusion of phosphorous along the sidewalls and gallium back diffusion from the droplet. All currents are calculated analytically as a function of droplet geometry. Complementary experiments are performed to extract the two model parameters governing the diffusion currents. We then compute numerically the dynamics of the system exposed to a constant external phosphorous flux. Our quantitative model allows one to predict how droplet contact angle and radius change while operating blindly in a standard epitaxy chamber. Controlling these parameters is crucial for tailoring the crystal phase of III-V nanowires and fabricating quantum size structures.

INTRODUCTION

Nanowires (NWs) of III-V semiconductors, with diameters of a few tens of nanometers and lengths up to several micrometers, have remarkable physical properties which open large prospects of original applications.[1–5] Many of these however require a precise control of the NW geometry. This is for instance the case in devices relying on quantum confinement, which can be obtained by inserting thin disks along the NW axis; in addition, lateral confinement may occur in very thin NWs.[6,7]

To produce III-V NWs, the vapor-liquid-solid (VLS) method[8] is often used. In this growth mode, the catalyst droplet located at the top of the NW acts as a reservoir of constituents which favors nucleation and feeds the growth of the NW. It also sets the NW diameter, and its composition in the case of alloys. Moreover, the contact angle of the droplet impacts the crystal structure of the NW.[9–11] Therefore, controlling the droplet volume and geometry is crucial to obtain NWs with required dimensions and crystal structure.

For GaAs and GaP, with exciton Bohr radii of about 15 and 5 nm, respectively, lateral confinement typically occurs for NW diameters below 10 to 30 nm. This requires droplets with similar sizes. Unfortunately, forming such small

droplets on the surface of the growth substrate is challenging. Nevertheless, VLS growth makes it possible to modify the droplet geometry by tuning the growth fluxes. In particular, in order to reduce locally the NW diameter, one can consume partially the droplet during growth.[12,13]

Self-catalyzed growth[14–19] is a variant of III-V VLS growth, whereby the catalyst droplet contains only the NW elemental constituents, and actually a very large proportion of the group III species.[20] It presents several advantages, such as a reduced risk of contamination of the NW by foreign impurities and the possibility to attain a stationary NW radius.[19,21,22] The method is particularly suited to control the NW geometry. Since the catalyst droplet contains no foreign atoms, its volume can be reduced at will. It can even be consumed completely in order to inhibit VLS growth in favor of vapor-solid (VS) growth, which is useful to form shells of controlled thickness. Without going to such extremes, the droplet diameter can be reduced to obtain very thin NWs.[13]

In practice, the droplet volume is controlled by changing the ratio of the group III and group V fluxes. An excess input of group III inflates the droplet whereas an excess of group V reduces its volume by consuming stored group III atoms to form the III-V solid phase. This may change the droplet contact angle, the droplet radius, or both. There is thus a strong interest in understanding the dynamics of droplet consumption in order to control precisely the geometry and the crystal phase of the NW.

In the present work, we combine experiments and theory to clarify and tailor the mechanisms of droplet consumption. We develop a model which describes the evolution of a Ga catalyst droplet on top of a GaP NW. This model can easily be transposed to other self-catalysed III-V NWs. We consider the usual case of droplet consumption by providing only group V atoms. We deal with low-density NW arrays, where the shadowing by neighboring NWs can be neglected. We establish the mechanisms that empty the droplet and estimate their respective contributions to the consumption process, which are all given in analytical form. This allows us to predict the droplet evolution under group V exposure. This understanding of the droplet dynamics is particularly important since direct and real-time observation of these processes is not accessible in standard epitaxy systems; on the other hand, *in situ* studies do provide such data, but at the expense of a different NW environment.[10,11]

EXPERIMENTS

Preparation of the patterned growth substrates

We prepared patterned growth substrates as follows. A 33 nm thick silica layer was formed on fully deoxidized intrinsic Si(111) wafers by chemical vapor deposition. The hexagonal pattern, which comprised several areas with pitches of 300, 400, 500 nm, 1 and 5 μm, was written in a polymethyl methacrylate (PMMA) mask over the silica. For each pitch, holes with diameters from 30 to 70 nm were then drilled in the silica layer using reactive ion etching by CHF_3/SF_6. However, only NWs grown from holes of diameter 50 nm were used in our quantitative analysis. The PMMA resist was removed by using acetone and isopropanol. Finally the silica was cleaned by an oxygen plasma. Immediately before introduction into the growth system, the substrate was etched with 1% HF for 30 s to obtain a completely deoxidized Si(111) surface at the bottom of the holes. The samples were outgassed before growth in a separate chamber at 600°C and further outgassed *in situ* at 680°C.

Nanowire growth

Self-catalyzed GaP nanowires were grown by molecular beam epitaxy (MBE) in a RIBER 32 machine on the patterned substrates, at 600°C. Ga alone was first deposited for 2 min to form droplets in the holes. Ga and P_2 were then provided simultaneously for 20 min. The Ga flux was equivalent to a 2D growth rate of 0.144 nm s^{-1} for (100) GaP, as measured by reflection high energy electron diffraction (RHEED). The P_2 flux was adjusted as follows. Using

RHEED, we first found the value F_0 corresponding to the transition between group-III-limited and group-V-limited growth on (100) GaP, where the effective atomic fluxes of both species are equal, as described previously for GaAs.[16,23,24] For growth, we adjusted it to $1.3F_0$ and kept the same Ga flux. The substrate was rotated (at a rate of 20 to 30 rpm) during growth and droplet consumption.

Droplet consumption

After growth, to consume the catalyst droplet, the Ga flux was abruptly switched off and the sample exposed to P_2 only. The atomic flux of phosphorous was then set to about 2.3 times the flux used during growth, *i.e.* 1.07×10^{19} at m^{-2} s^{-1}. The experiment was terminated by closing all shutters and valves abruptly and switching off the substrate heater for rapid cooling. The duration of exposure to phosphorous was varied between 1 min and 3 min in order to study the progress of the catalyst droplet consumption. The NW arrays were observed by scanning electron microscopy (SEM) in a FEI Magellan system operated at 10 kV.

Before droplet consumption, our arrays of as-grown NWs are of high quality (Fig. 1(a)). Except for a small fraction (where we find 3D crystallites), all openings are occupied by single vertical NWs, which are slightly reverse-tapered, their radius varying from 40-45 to 55-60 nm from bottom to top (Fig. 1(a)). Table 1 indicates how the geometry of NWs and droplet vary with pitch. Importantly, no significant difference is observed between the largest pitches of 1 and 5 μm.

Figure 1(b) to (f) illustrates the droplet geometry after different times of consumption by exposure to phosphorus. The consumption rate is not the same for all pitches. In arrays with pitches of 500 nm and less, the droplets are consumed more slowly than in arrays with larger pitches. However, as was the case for the NW growth rate, we observed very little difference in consumption rate for pitches of 1 μm and larger (figures are given below). This indicates an influence of neighboring NWs in dense arrays

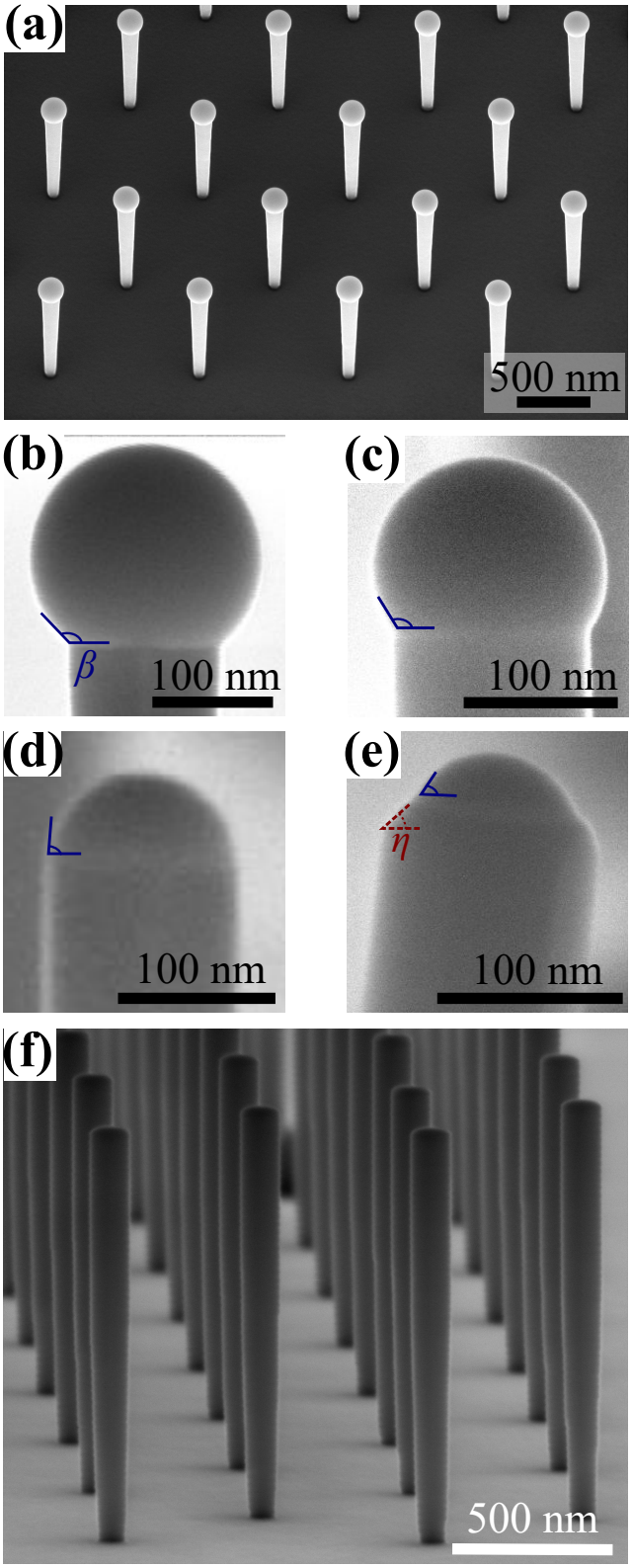

Figure 1: SEM images of GaP NWs (from arrays with 1 μm pitch) after various times of droplet consumption. (a) General view of an array. The apical droplet immediately after growth (b) and after being consumed for 1 min (c), 2 min (d) and 2 min 20 s (e). Droplet contact angle β and tapering angle η of terminal section are indicated. (f) An array with totally consumed droplets.

and the absence of interaction in arrays with distant NWs. This can be related to the small inclination angle $\alpha = 17°$ of the P source with respect to the substrate normal, which restricts shadowing to the close neighborhood of each NW. We will show that a significant amount of phosphorous reaches the droplet after being re-emitted from the neighboring surfaces, so that the presence of the NWs close by could have a strong influence on this flux. The impact of the neighboring NWs, which was studied previously in the context of growth,[25,26] is out of the scope of the present work. Instead, we focus on large pitches and model a single NW isolated on its substrate.

Table 1: Measured morphologies of self-catalysed GaP NWs grown in arrays with various pitches. H_{NW}: NW height, R_{NW}: top NW radius, β: droplet contact angle.

Pitch (nm)	400	1000	5000
H_{NW} (nm)	680 ± 21	725 ± 20	726 ± 22
R_{NW} (nm)	50 ± 2	58 ± 3	60 ± 2
β (°)	138 ± 2	137 ± 2	137 ± 2

Nevertheless, using arrays with a high yield of vertical NWs presents several advantages. It insures that all NWs grow in the same conditions. A NW extracted at random for TEM examination is very likely representative of the ensemble and we are sure that it did not have any neighbor closer than the pitch, as necessary to employ our isolated NW calculations. Anyway, most measurements are performed with NWs still in position, using SEM images where the local environment is readily checked.

The droplet geometry is described by two parameters which may change over time, namely its contact angle β and its base radius. The evolution of the droplet can be divided into three stages corresponding to different regimes of variation of these parameters. Initially, β is around 137° (Fig. 1(b) and Table 1). During consumption, as long as β remains larger than 90°, the droplet keeps a base radius equal to the NW radius (Fig. 1(c)). This will be called stage I. Once the contact angle reaches $\beta \simeq 90°$ (Fig. 1(d)), the NW tapers via the creation of sidewall facets tilted by angle $\eta \simeq 47°$ (Fig. 1(e)), a value close to that measured *in situ* by Panciera *et al.* for GaAs during droplet manipulation[11] (this tapering is much more pronounced than during stem growth, and in the opposite direction). The droplet remains pinned to the edge of these facets, so that its base shrinks in a known fashion while the contact angle keeps decreasing (stage II). We did not observe any contact angle below 63°. This value is close to the Young's angle $\beta_Y \simeq 65°$ for a pure Ga liquid droplet on a GaP (111) surface.[27] After the droplet adopts the Young's contact angle (stage III), it depins from the tilted facets, its base diameter shrinks further until it finally vanishes (Fig. 1(f)). The tapering of the nanowire top end is clearly visible in Figure 1(e), whereas it is much reduced after complete droplet consumption (Fig. 1(f)). Reduced tapering and flat nanowire top are consistent with a transfer, at stage III, of the Ga of the vanishing droplet to the periphery of the top of the nanowire to form GaP by radial VS growth.

MODEL AND CALCULATIONS

Calculations of the various contributions to droplet consumption

To describe the dynamics of the droplet geometry during crystallization, we develop calculations taking into account four possible channels of droplet consumption under exposure to the sole group V species (Fig. 2). Three channels correspond to different currents of phosphorus to the droplet that consume gallium by forming solid GaP. Phosphorus atoms can indeed be delivered to the droplet by direct impingement of the beam (i), or after re-emission from the substrate (ii) or via surface diffusion of adatoms deposited on the substrate or on the sidewalls (iii). This third pathway is usually deemed ineffective for group V elements. Finally, the droplet may shrink due to back diffusion of Ga atoms down the NW sidewalls (channel (iv)).

To calculate the corresponding currents

(number of atoms per unit time), we consider an axisymmetric NW isolated on an infinite substrate. The apical droplet is a spherical cap with contact angle β, radius R_d and base radius $R_b = R_d \sin\beta$ and the NW stem a right circular cylinder with radius R_{NW} and height H_{NW} (Fig. 2). As long as the droplet remains pinned to the sidewalls, $R_b = R_{NW}$. The whole system is exposed to a P_2 molecular beam (at angle α), yielding an atomic P flux F_e per unit area of substrate.

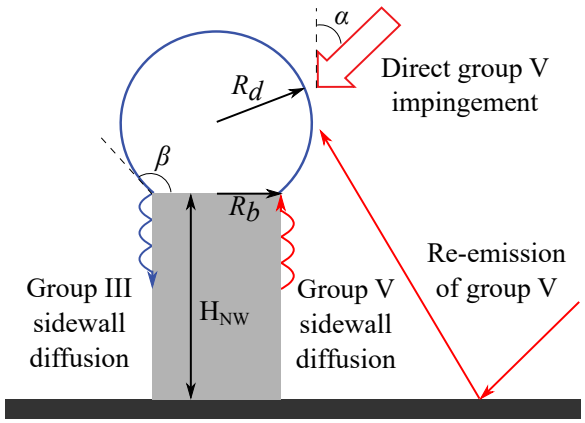

Figure 2: Schematics of the material currents contributing to the consumption of a droplet located on top of an isolated III-V NW. Here, $R_b = R_{NW}$.

(i) Glas has calculated the direct current I_{dir} to a spherical cap droplet.[28] It depends on droplet geometry and on beam orientation via a certain function $\varepsilon(\alpha, \beta)$:

$$I_{dir} = \pi R_b^2 F_e \, \varepsilon(\alpha, \beta) \tag{1}$$

(ii) Several authors have considered that both group III[26,29,30] and group V species[16,20] can be transferred to the NW sidewalls and to the droplet by re-emission of atoms initially landed on the substrate or on the neighboring NWs, a process sometimes called secondary adsorption. Ramdani *et al.* showed that As re-emission can contribute significantly to GaAs NW growth.[16] Here, for our isolated GaP NW, we consider re-emission of phosphorous from the substrate only. The absence of deposit on the mask indicates that all P species that reach it are actually re-emitted.

To calculate I_r, we need to specify the *a priori* unknown angular distribution of re-emission. We test two hypotheses, already considered for various purposes in the literature, namely Lambertian (cosine) distribution[26,31,32] and specular reflection.[16,26] In the former case, the phosphorous species are re-emitted independently of their incidence angle. In the latter, they are reflected by the substrate at an angle equal to their fixed incidence angle α. These are two extreme cases: specular re-emission corresponds to a purely mechanical interaction with the substrate whereas a Lambertian distribution is expected for molecules having reached equilibrium with it.[33,34] In both cases, we assume that re-emission occurs at the point of incidence, thereby neglecting surface diffusion on the mask.

In the Lambertian case (superscript L), the current re-emitted, per unit area of substrate and unit solid angle, is $\pi^{-1} F_e \cos\theta$. The analytical calculation of the total P current I_r^L re-emitted to the droplet is given in Supporting information S1. For $\beta \geq \pi/2$, we derive three analytical approximations:

$$I_{r,i}^L = \frac{\pi}{2} F_e R_d^2 \left[(1 - \cos\beta)^2 - I_i(\beta) \right] \tag{2}$$

where the I_i terms, given by Eqs. (S2.12), (S2.16), (S2.17) for $i = 1, 2, 3$, are alternative corrections accounting for a partial blockage of re-emission by the NW stem. These approximations (all more precise than a previous proposal[32]) are discussed below. If $\beta \leq \pi/2$, I_r^L is given exactly by Eq. (2) with $I_i = 0$.

In the specular case (superscript S), re-emission is calculated using the method previously applied to the direct current[28] or as shown in Supporting information S2, which gives:

$$I_r^S = \frac{F_e R_d^2}{\cos\alpha} \begin{cases} \beta + \sin\beta\cos\beta\,(1 - 2\sin\alpha) \\ \quad -\frac{\pi}{2}\cos\alpha\sin^2\beta \quad \text{for } \beta \geq \frac{\pi}{2}; \\ \\ \frac{\pi}{2} - \cos\beta\sqrt{\sin^2\alpha - \cos^2\beta} \\ \quad -\sin^2\beta\cos\alpha\arccos(\cot\alpha\cot\beta) \\ \quad -\arcsin\frac{\cos\beta}{\sin\alpha} \quad \text{for } \frac{\pi}{2} - \alpha \leq \beta \leq \frac{\pi}{2} \end{cases} \tag{3}$$

with $I_r^S = 0$ for $\beta \leq \pi/2 - \alpha$.

Figure 3 gives the variations of the direct and re-emitted currents calculated in the Lamber-

tian and specular cases, as a function of the droplet contact angle β, for the P_2 beam incidence $\alpha = 17°$ pertaining to our experiments, and for arbitrary incidence $\alpha = 45°$, for comparison. For Lambertian re-emission, corrections I_1 and I_2 (Eq. (2)) give very close results. This is manifest in the main panel of Fig. 3 but also in the insert, where we compare the absolute values of I_1 and I_2 as a function of contact angle. The closeness of these terms for any beta is very satisfying since, as shown in Supporting information S1, they yield an overestimate and an underestimate of the re-emitted current, respectively. Hence, the real current, which lies in between, is very well approximated by either. For specificity, we shall use I_1. On the other hand, the insert shows that the correction may amount to more than 10% of the total for contact angles on the order of those encountered at the start of consumption, which makes it necessary.

In Figure 4(a-c), the experimental variations over time of several geometrical parameters of the droplet (symbols) are compared to various calculations (lines). The measured droplet contact angle, radius and volume decrease more rapidly than those calculated by including only direct impingement (i) and re-emission (ii), whether Lambertian or specular (broken curves). These two currents do not provide enough phosphorous to consume the droplet and the missing amount is significant.

This leads us to consider the two extra channels of Ga consumption mentioned above. The first one (iii) consists in a third P current into the droplet, due to migration up the sidewalls. Whereas NW growth models commonly take into account the surface diffusion of group III atoms,[35,36] that of the volatile group V species is usually neglected.[12,13,16,19,37] Several authors nevertheless discuss it[24,38] and some even estimated As diffusion lengths up to hundreds of nm at usual growth temperatures.[39]

To obtain the phosphorous diffusion current (iii), we introduce a surface diffusion length λ_V and simply assume that all atoms impinging the sidewalls within a distance λ_V below the TPL are transferred to the droplet. This implies that $H_{NW} > \lambda_V$, which also excludes any contribution from diffusion on the substrate. We thus only need to calculate the direct and re-emitted currents collected by the sidewalls.

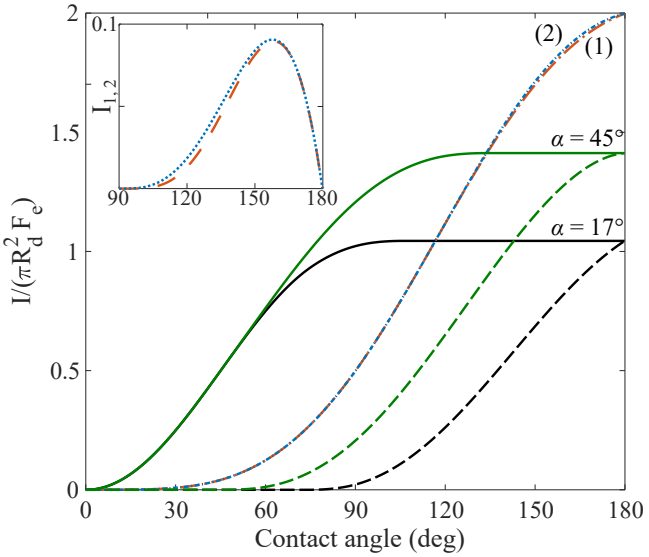

Figure 3: Currents of group V species collected by the droplet as a function of its contact angle β: direct contribution (full curves) and re-emission in the specular (dashes) or Lambertian (dash-dots) cases. Direct and specularly re-emitted currents are given for the two incident beam angles $\alpha = 17°$ (black) and $\alpha = 45°$ (green). Lambertian re-emission is calculated within approximations (1) (loose dash-dots) and (2) (dense dash-dots). All currents are normalized by sphere section πR_d^2 and material source flux F_e. Inset: Variation with contact angle β of terms I_1 (Eq. (S2.12) with $J_1 = 0$, dashes) and I_2 (Eq. (S2.16), dots), which correct Lambertian re-emission for stem blockage.

The direct current is that intercepted by a vertical rectangle of width $2R_{NW}$ and height λ_V, namely $I_{dir} = 2F_e R_{NW} \lambda_V \tan\alpha$. In case of specular reflection, the re-emitted current is the same, which gives a total P diffusion current

$$I_{dif}^S = 4F_e R_{NW} \lambda_V \tan\alpha \qquad (4)$$

For Lambertian re-emission, the calculation (Supporting information S3) is exactly the same as performed previously in the context of NW heating by Glas and Harmand[40] and gives

$$I_{dif}^L = F_e R_{NW} \lambda_V \left(2\tan\alpha + \pi\right) \qquad (5)$$

The second extra consumption channel, non exclusive of the first one, does not involve phos-

phorous, but back diffusion of Ga atoms out of the droplet (iv). To calculate this contribution, we use the transition state approach developed for NW growth by Krogstrup *et al.*[39] The net group III current is the difference of the currents entering and leaving the droplet. The former scales with the density of Ga adatoms on the sidewalls, just below the TPL, and depends exponentially on their chemical potential (with respect to the transition state energy). However, due to the lack of external Ga supply during droplet consumption, density and hence chemical potential should be low. We thus consider only the reverse transition liquid $\rightarrow$ adatom. We show in Supporting information S4 that this back diffusion current can be expressed as:

$$I_{bd} = 2\pi R_b \; A(T) \exp\left(\frac{\mu_{GT}}{k_B T}\right) \qquad (6)$$

with μ_{GT} a Gibbs-Thomson correction, to be evaluated at each step of the consumption process.

The droplet also suffers from desorption of its two constituents, with opposite effects on its consumption. However, Supporting information S5 shows that we can safely ignore these pathways in our calculations, at least for the present experiments.

Computation of droplet dynamics

The number $dN_V/dt = I_{dir}+I_r+I_{dif}$ of P atoms entering the droplet per unit time is obtained from the previous calculations, with I_r and I_{dif} calculated either for Lambertian (Eqs. (2),(5)) or specular (Eqs. (3),(4)) re-emission. Assuming that these atoms are all used to form GaP, this consumes the same number of Ga atoms stored in the droplet, which volume thus decreases by $dV_i = dN_V \; \omega_{Ga}^L$. In addition, $dN_{III}/dt = I_{bd}$ Ga atoms leave the droplet per unit time by back diffusion, which reduces its volume by an extra $dV_{bd} = dN_{III} \; \omega_{Ga}^L$. The droplet volume V_d thus obeys equation

$$\frac{dV_d}{dt} = \frac{dV_i}{dt}(\beta, R_b) + \frac{dV_{bd}}{dt}(\beta, R_b) \qquad (7)$$

where we stress that all currents depend on the instantaneous geometry of the droplet, defined by contact angle β and base radius R_b. However, a given decrease of droplet volume may be effected via a change of β or R_d, or both, and our model does not prescribe which particular combination of these changes will actually occur. To lift this ambiguity, we use our experimental results which, as described above, allow us to divide the droplet consumption process into three main stages. During stage I, R_b remains equal to R_{NW} and V_d decreases entirely via a decrease of β. Stage I ends when β reaches about $\pi/2$. Then (stage II), the NW starts tapering but the droplet remains pinned to the edge between tilted and top facets; we assume a fixed tapering angle $\eta = 47°$ (Fig. 1(e)). During this stage, R_b and β both vary. After β reaches the Young's angle β_Y, it remains fixed to this value but the droplet depins so that R_b shrinks and its volume further decreases until vanishing (stage III). Once this is specified, our recursive procedure allows us to model self-consistently the evolution of the droplet parameters β and R_d during consumption, according to Eq. (7).

This succession of stages is not based only on our *ex situ* observations and is not specific to GaP. Indeed, Panciera *et al.*, recently investigating the self-catalyzed growth of GaAs NWs by *in situ* TEM, observed the very same regimes when making the droplet swell or shrink by varying the V/III flux ratio[11] (these experiments were subsequently modelled, without accounting analytically for all pathways considered here[41]). Various *ex situ* observations had previously showed a tapered section near the top of the NW associated with a group-V-rich regime and a flat top facet after total droplet consumption,[12,13,42,43] although others did not detect tapering.[37]

On this basis, we solve numerically Eq. (7) using the *MATLAB* environment, with a time step of 0.01 s. At each step k, the four currents contributing to droplet consumption are calculated by using our analytical expressions, evaluated for the instantaneous droplet geometry, defined by parameters $\beta(k)$, $R_d(k)$. The droplet volume V_d at step $k+1$ is then computed and parameters $\beta(k+1)$, $R_d(k+1)$ yielding this volume are selected depending on the current stage of the process (I, II or III), as

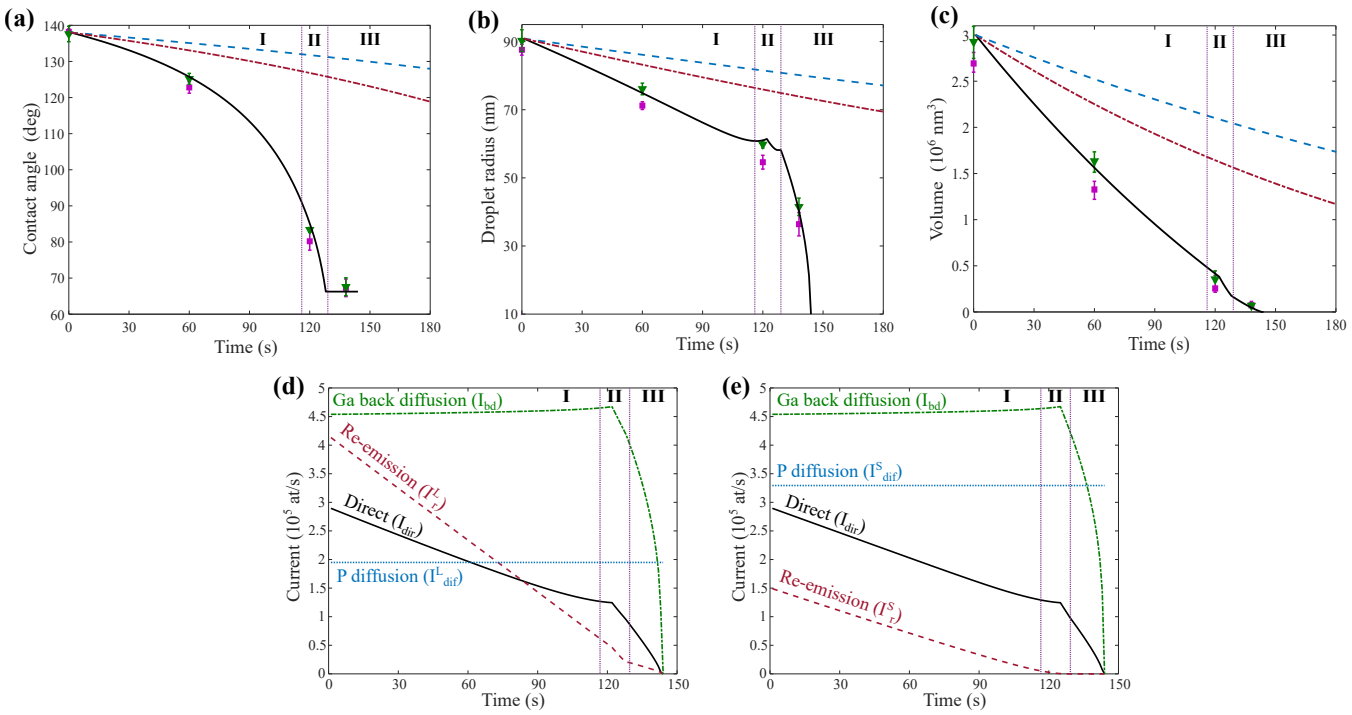

Figure 4: (a-c) Variations of droplet contact angle β (a), radius R_d (b) and volume V_d (c) during droplet consumption. Symbols give the experimental values for pitches of 1 μm (squares) and 5 μm (triangles), averaged over several NWs. The curves show the results of calculations considering only direct impingement and re-emission [specular (dashed) or Lambertian (dash-dotted)], or with phosphorous and gallium diffusion in addition (full curve). (d,e) Variations during droplet consumption of direct (I_{dir}), re-emitted ($I_r^{L(S)}$) and diffusion ($I_{dif}^{L(S)}$) currents of P and of Ga back diffusion current (I_{bd}), calculated under assumptions of Lambertian (d) or specular (e) P re-emission from the substrate.

discussed above. This process is repeated until the droplet vanishes ($V_d = 0$). We discuss in Supporting information S6 in which measure these expressions, derived for a droplet pinned at the TPL of a cylindrical NW (as pertains to stage I), can still be used in altered geometries at stages II (NW tapering) and III (droplet depinning).

Determination of the model parameters

Our model includes two unknown parameters, namely the P diffusion length λ_V (Eqs. (4), (5)) and prefactor $A(T)$ for Ga back diffusion (Eq. (6)). To estimate these parameters, we devised complementary experiments based on the following remarks. During consumption, the Ga atoms lost by the droplet can either generate an axial solid volume V_{ax} by VLS growth, or diffuse to the sidewalls to form a radial volume V_{rad} by VS growth (Fig. 5(g)). Since the droplet is the only source of Ga, V_{ax} should correspond to the total phosphorous current $I_{dir} + I_r + I_{dif}$ arriving to the droplet and V_{rad} to the Ga back diffusion current I_{bd}.

We performed specific experiments, at the same temperature, to measure these volumes. To this end, we insert 5 Ga(As,P) marker layers (each grown for 10 s) separated by GaP segments (grown for 50 s) at the end of growth. After the growth of a similar final GaP segment, the droplet is totally consumed by exposing the system to P only. Individual NWs were studied by transmission electron microscopy (TEM) in a FEI Titan microscope operated at 200 kV. We recorded high-angle annular dark field (HAADF) images, where the Ga(As,P) alloy appears brighter than GaP, due to a higher average atomic number. The HAADF images clearly show the markers (Fig. 5(a-c)) but also reveal a $2-3$ nm-thick bright shell below the last marker (Fig. 5(c)), indicative of a small Ga(As,P) radial growth during axial marker

growth. These thin lines extend down to the bottom of the NW (Fig. 5(c-e)).

The droplet consumption results in the growth of a top segment with length of about 4 to 4.5 R_{NW} (Fig. 5(b)). Its radius is almost equal to that of the last Ga(As,P) marker (it only diminishes slightly at the very top due to shrinking of droplet base at the end of consumption). This implies that this top segment is grown in the VLS mode, without any significant radial VS growth, and thus corresponds to V_{ax}. In addition, a GaP shell forms. Below the last marker, its inner border is clearly delineated by the thin Ga(As,P) shell formed before consumption. Panels (b) and (c)-(e) in Figure 5 show that the thickness of this outer shell varies from a few nm at the markers level to 13−15 nm at the NW foot. Its formation during droplet consumption (under P only) is confirmed by energy dispersive X-ray (EDX) analysis which clearly shows As-containing vertical traces corresponding to the inner Ga(As,P) shell, while no As is detected in the outer part of the shell (Fig. 5(f)). Note that a back-diffusion of Ga all the way down to the NW foot, *i.e.* along 1.4 to 1.6 μm, is compatible with estimates of Ga diffusion lengths of several microns during MBE growth of III-V NWs[19,39,44] but not with the short diffusion lengths reported for GaP NWs.[45]

An analysis of the volumes grown during droplet consumption shows that $96 \pm 4\%$ of the initial droplet volume V_0 is transformed into solid GaP. More precisely, we measure $V_{ax} = (0.53 \pm 0.03)\, V_0\, \tilde{\omega}$ and $V_{rad} = (0.44 \pm 0.05)\, V_0\, \tilde{\omega}$ (see Supporting Information S7), where $\tilde{\omega} = \omega_{GaP}/\omega_{Ga}^{L}$ accounts for the fact that each Ga atom from the liquid yields a Ga-P pair (of volume ω_{GaP}) in the solid. Here, V_0 is obtained from the narrowly distributed contact angle β_0 measured on samples removed from the growth chamber immediately after growth, before droplet consumption (Fig. 1(b), Table 1).

Recovering as solid GaP nearly the exact amount of liquid Ga estimated to be present in the droplet before its consumption strengthens our estimate of V_0. This confirms that no significant loss of Ga occurs during rapid post-growth cooldown and that β_0 is actually the contact angle at the end of NW growth.

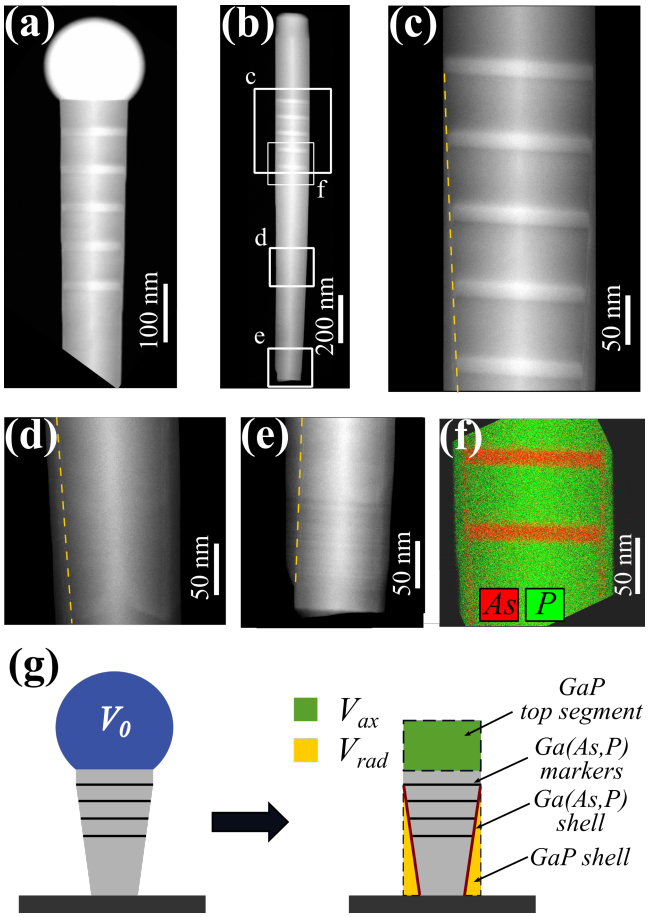

Figure 5: GaP NWs with Ga(As,P) marker layers inserted before droplet consumption. (a-e) HAADF TEM images. (a) A NW before droplet consumption. The markers appear brighter than GaP. (b) A NW after total droplet consumption. (c-e) Images of the areas indicated by the same letters in (b), showing the formation of a GaP shell along the whole NW. Dashed lines drawn at the left mark the interface between initial NW and shell. (f) Map of group V composition obtained by EDX spectroscopy over area (f) of panel (b), showing markers and the thin As-containing shell parallel to NW axis. (g) Schematics of the evolution of the NW during droplet consumption, resulting in simultaneous axial and radial growth, with markers shown as black lines and inner Ga(As,P) shell shown as red lines.

This experiment allows us to measure the value of prefactor A of Eq. (6). Namely, for back diffusion to provide the amount of Ga necessary to form volume V_{rad}, we must have $A = 6.85 \times 10^8$ at nm^{-1}s^{-1} at 600°C.

As regards axial growth, neither Lambertian nor specular re-emission, together with the di-

rect current, provide enough phosphorous to create the observed volume V_{ax} by VLS growth. The direct and re-emitted P currents consume only 37% and 23% of V_0 (*i.e.* 70% and 43% of V_{ax}) in the Lambertian and specular cases, respectively. What remains of V_{ax} has to be formed using phosphorous provided by sidewall diffusion. This requires phosphorous diffusion lengths λ_V of 80 nm and 400 nm for Lambertian and specular re-emission, respectively.

The relative values of V_{ax} and V_{rad} must depend on the radius of the NW analyzed. However, parameters λ_V and A are expected to depend only on temperature. We can thus now use the values quoted above to model self-consistently the evolution of the droplet geometry at the same temperature, during the three stages of the consumption process, namely (I) $\beta \geq \pi/2, R_b = R_{NW}$, (II) $\beta_Y \leq \beta \leq \pi/2$, with R_{NW} and R_b decreasing according to tapering angle η, and (III) $\beta = \beta_Y$, R_b decreasing further. From now on, all calculations are carried out using input parameters corresponding to our growth conditions, with $R_{NW} = 60$ nm.

RESULTS AND DISCUSSION

The full curves in Figure 4(a-c) illustrate the evolution of droplet contact angle, radius and volume with time, when all three phosphorus pathways (direct impingement, re-emission, diffusion) are active, together with Ga back diffusion. It appears that, at variance with the calculations omitting diffusion, these four currents consume the right amount of Ga to account for our experimental data (symbols in Fig. 4(a-c)). During stage I, as prescribed by the experiments and taken as constraints in our calculations, the volume of the droplet can only change via a reduction of the contact angle, and during stage III via a shrinking of its base. At stage II, the droplet behavior is more complex since β and R_b vary simultaneously.

It is interesting to analyze the droplet fractions consumed in the different possible ways. Figure 4(d,e) shows the evolution of each current with time during consumption. For large contact angles, at the beginning of consumption, the contributions from the four material pathways are of the same order. With decreasing contact angle, the phosphorous impingement currents (i,ii) diminish (re-emission even vanishes in the specular case), making Ga and P diffusion (which are β-independent except for weak small size effects at very small R_b) the most effective mechanisms for emptying the droplet. During stages II and III, Ga back diffusion diminishes due to the decrease of R_b but P diffusion remains constant (see also Supporting information S6). Overall, with either Lambertian or specular re-emission, the diffusion of both species accounts for around two thirds (63% and 76%, respectively) of droplet consumption. Ga back diffusion contributes significantly. The corresponding current (Eq. (6)) depends only on droplet base radius and temperature, whereas the phosphorous currents (Eqs. (1)-(5)) all scale with external flux F_e. Thus, increasing the phosphorous supply will increase the contribution of direct and re-emitted currents. In Figure 4(d,e), the currents are calculated for our already quite high experimental P flux (corresponding planar growth rate is about 0.44 nm s^{-1}). Increasing *e.g.* this flux five times, Ga back diffusion still contributes significantly, for about 15% of the total. On the other hand, an accurate control of droplet geometry requires low consumption rates and, therefore, low phosphorous fluxes. Another option would be to reduce Ga back diffusion, which might be achievable by lowering temperature, but this requires a separate study.

Our model predicts accurately the consumption time needed to obtain a droplet with predefined geometry. Stopping the process at a very small base radius might be tricky however, since $R_b = R_d \sin\beta$ decreases rapidly when it gets small (Fig. 4, stage III), even though Ga is then mostly consumed via back diffusion (which decreases with R_b). Another difficulty in achieving a given droplet size might stem from the residual group V species that linger in the MBE chamber even after the closure of all valves and shutters.[46]

We performed all calculations under two alternative re-emission hypotheses. As seen in

Fig. 3, at least for group V beam incidence α below 45° (which accounts for most MBE setups), specular reflection delivers a much lower current to droplets with large contact angle. Moreover, Lambertian re-emission operates until total consumption of the droplet. However, we cannot state which is the actual scheme, since our experiments can be fitted with both, albeit using very different P diffusion lengths. The value $\lambda_V \simeq 400$ nm found for specular re-emission, about five times the Lambertian value, seems unlikely large. Since the specular re-emission currents depend on the source inclination angle whereas the Lambertian currents do not, performing experiments at different source angles might clarify this question.

CONCLUSIONS

In summary, we developed a model of the consumption of a group III droplet seating on top of a III-V NW when only group V atoms are provided. Our model is based on series of experiments on Ga droplets on top of self-catalyzed GaP NWs, exposed to P. We find that, beside the direct impingement of group V species and their re-emission from the substrate, group V diffusion to the droplet and group III back diffusion from the droplet, along the NW sidewalls, both contribute significantly to the consumption process and we established a general method to measure the parameters governing these two fluxes. We derived analytical expressions for all re-emitted and diffusion currents as a function of instantaneous droplet geometry, which we then used to model the decrease of the droplet volume over time. Our experimental data can only be correctly fitted if the four consumption pathways are included.

Our model allows one to predict the time needed to reduce the droplet to a given geometry, under given group V flux and starting from a known geometry. Controlling the droplet contact angle is key to selecting at will the crystal phase of III-V NWs[11] and fabricating crystal phase heterostructures.[47–49] On the other hand, lateral confinement in radial heterostructures requires tailoring the droplet base radius. While dedicated *in situ* TEM experiments offer unprecedented opportunities to achieve such control in a single NW, it is highly desirable to attain the same objectives reproducibly and blindly in arrays of identical NWs grown on a crystalline substrate in a standard epitaxy equipment. Our model, which is generic at least for III-V NWs, grants such control, in particular by predicting precise timings for the two extreme stages of consumption, where one of the two geometrical parameters of the droplet (contact angle or base radius) varies while the other remains constant.

Supporting Information Available

S1,S2: Calculation of the atomic current re-emitted from substrate to droplet, in the cases of Lambertian and specular re-emissions. S3: Calculation of the atomic current re-emitted from substrate to NW sidewalls, in the case of Lambertian re-emission. S4: Calculation of gallium back diffusion. S5: Desorption of P and Ga from the droplet. S6: Using our analytical expressions of the atomic currents in case of NW tapering or droplet depinning. S7: Experiments with marker layers (PDF)

Acknowledgement This research has received funding from the European Union's Horizon 2020 research and innovation programme under the Marie Skłodowska-Curie grant agreement No 722176 (INDEED network), from ANR, the French National Research Agency, within project "Engineering spins and photons from anisotropic dots in NWs" (ESPADON, grant ANR-15-CE24-0029-01) and from the French RENATECH network (Réseau français de nanofabrication). The authors also thank Federico Panciera (C2N) for sharing some of his unpublished data.

References

(1) Krogstrup, P.; Jorgensen, H. I.; Heiss, M.; Demichel, O.; Holm, J. V.; Aagesen, M.; Nygård, J.; Fontcuberta i Morral, A.

Single-nanowire solar cells beyond the Shockley–Queisser limit. *Nature Photon.* **2013**, *7*, 306–310.

(2) Frederiksen, R. S.; Alarcon-Llado, E.; Krogstrup, P.; Bojarskaite, L.; Buch-Manson, N.; Bolinsson, J.; Nygård, J.; Fontcuberta i Morral, A.; Martinez, K. L. Nanowire-aperture probe: Local enhanced fluorescence detection for the investigation of live cells at the nanoscale. *ACS Photon.* **2016**, *3*, 1208–1216.

(3) Saket, O.; Himwas, C.; Piazza, V.; Bayle, F.; Cattoni, A.; Oehler, F.; Patriarche, G.; Travers, L.; Collin, S.; Julien, F. H. et al. Nanoscale electrical analyses of axial-junction GaAsP nanowires for solar cell applications. *Nanotechnology* **2020**, *31*, 145708.

(4) Haffouz, S.; Poole, P. J.; Jin, J.; Wu, X.; Ginet, L.; Mnaymneh, K.; Dalacu, D.; Williams, R. L. Single quantum dot-in-a-rod embedded in a photonic nanowire waveguide for telecom band emission. *Appl. Phys. Lett.* **2020**, *113102*, 021603.

(5) Motohisa, J.; Hara, S. In *Fundamental properties of semiconductor nanowires*; Fukata, N., Rurali, R., Eds.; Springer: Singapore, 2021; pp 371–431.

(6) Kammhuber, J.; Cassidy, M. C.; Zhang, H.; Önder Gül,; Pei, F.; de Moor, M. W. A.; Nijholt, B.; Watanabe, K.; Taniguchi, T.; Car, D. et al. Conductance quantization at zeromagnetic field in InSb nanowires. *Nano Lett.* **2016**, *16*, 3482–3486.

(7) Barrigón, E.; Heurlin, M.; Bi, Z.; Monemar, B.; Samuelson, L. Synthesis and applications of III–V nanowires. *Chem. Reviews* **2019**, *119*, 9170–9220.

(8) Wagner, R. S.; Ellis, W. C. Vapor-liquid-solid mechanism of single crystal growth. *Appl. Phys. Lett.* **1964**, *4*, 89–90.

(9) Glas, F.; Harmand, J.-C.; Patriarche, G. Why does wurtzite form in nanowires of III-V zinc blende semiconductors? *Phys. Rev. Lett.* **2007**, *99*, 146101.

(10) Jacobsson, D.; Panciera, F.; Tersoff, J.; Reuter, M. C.; Lehmann, S.; Hofmann, S.; Dick, K. A.; Ross, F. M. Interface dynamics and crystal phase switching in GaAs nanowires. *Nature* **2016**, *531*, 317–322.

(11) Panciera, F.; Baraissov, Z.; Patriarche, G.; Dubrovskii, V.; Glas, F.; Travers, L.; Mirsaidov, U.; Harmand, J.-C. Phase selection in self-catalyzed GaAs nanowires. *Nano Lett.* **2020**, *20*, 1669–1675.

(12) Priante, G.; Ambrosini, S.; Dubrovskii, V.; Franciosi, A.; Rubini, S. Stopping and resuming at will the growth of GaAs nanowires. *Cryst. Growth Des.* **2013**, *13*, 3976–3984.

(13) Kim, W.; Dubrovskii, V.; Vukajlovic-Plestina, J.; Tütüncüoglu, G.; Francaviglia, L.; Güniat, L.; Potts, H.; Friedl, M.; Leran, J.-B.; Fontcuberta i Morral, A. Bistability of contact angle and its role in achieving quantum-thin self-assisted GaAs nanowires. *Nano Lett.* **2018**, *18*, 49–57.

(14) Jabeen, F.; Grillo, V.; Rubini, S.; Martelli, F. Self-catalyzed growth of GaAs nanowires on cleaved Si by molecular beam epitaxy. *Nanotechnology* **2008**, *19*, 275711.

(15) Colombo, C.; Spirkoska, D.; Frimmer, M.; Abstreiter, G.; Fontcuberta i Morral, A. Ga-assisted catalyst-free growth mechanism of GaAs nanowires by molecular beam epitaxy. *Phys. Rev. B* **2008**, *77*, 155236.

(16) Ramdani, M. R.; Harmand, J.-C.; Glas, F.; Patriarche, G.; Travers, L. Arsenic pathways in self-catalyzed growth of GaAs nanowires. *Cryst. Growth Des.* **2013**, *13*, 91–96.

(17) Glas, F. Comparison of modeling strategies for the growth of heterostructures

in III-V nanowires. *Cryst. Growth Des.* **2017**, *17*, 4785–4794.

(18) Dubrovskii, V. G. Understanding the vapor-liquid-solid growth and composition of ternary III-V nanowires and nanowire heterostructures. *J. Phys. D: Appl. Phys.* **2017**, *50*, 453001.

(19) Dubrovskii, V. G.; Glas, F. In *Fundamental properties of semiconductor nanowires*; Fukata, N., Rurali, R., Eds.; Springer: Singapore, 2021; pp 3–107.

(20) Glas, F.; Ramdani, M.; Patriarche, G.; Harmand, J.-C. Predictive modeling of self-catalyzed III-V nanowire growth. *Phys. Rev. B* **2013**, *88*, 195304.

(21) Dubrovskii, V. G.; Xu, T.; Díaz Álvarez, A.; Plissard, S. R.; Caroff, P.; Glas, F.; Grandidier, B. Self-equilibration of the diameter of Ga-catalyzed GaAs nanowires. *Nano Lett.* **2015**, *15*, 5580–5584.

(22) Tersoff, J. Stable self-catalyzed growth of III-V nanowires. *Nano Lett.* **2015**, *15*, 6609–6613.

(23) Faktor, D.; Vesely, M.; Harman, R. New method for III/V flux ratio calibration in MBE systems from arsenic pressure measurements. *J. Cryst. Growth* **1993**, *126*, 499–501.

(24) Rudolph, D.; Hertenberger, S.; Bolte, S.; Paosangthong, W.; Spirkoska, D.; Doblinger, M.; Bichler, M.; Finley, J. J.; Abstreiter, G.; Koblmuller, G. Direct observation of noncatalytic growth regime for GaAs nanowires. *Nano Lett.* **2011**, *11*, 3848–3854.

(25) Sibirev, N. V.; Tchernycheva, M.; Timofeeva, M. A.; Harmand, J.-C.; Cirlin, G. E.; Dubrovskii, V. G. Influence of shadow effect on the growth and shape of InAs nanowires. *J. Appl. Phys.* **2012**, *111*, 104317.

(26) Oehler, F.; Cattoni, A.; Scaccabarozzi, A.; Patriarche, G.; Glas, F.; Harmand, J.-C. Measuring and modelling the growth dynamics of self-catalyzed GaP nanowire arrays. *Nano Lett.* **2018**, *18*, 701–708.

(27) Sibirev, N. V.; Timofeeva, M. A.; Bol'shakov, A. D.; Nazarenko, M. V.; Dubrovskii, V. G. Surface energy and crystal structure of nanowhiskers of III–V semiconductor compounds. *Phys. Solid State* **2010**, *52*, 1531–1538.

(28) Glas, F. Vapor fluxes on the apical droplet during nanowire growth by molecular beam epitaxy. *Phys. Stat. Sol. B* **2010**, *247*, 254–258.

(29) Rieger, T.; Heiderich, S.; Lenk, S.; Lepsa, M. I.; Grutzmacher, D. Ga-assisted MBE growth of GaAs nanowires using thin HSQ layer. *J. Cryst. Growth* **2012**, *353*, 39–46.

(30) Krogstrup, P.; Popovitz-Biro, R.; Johnson, E.; Madsen, M. H.; Nygård, J.; Shtrikman, H. Structural phase control in self-catalyzed growth of GaAs nanowires on silicon (111). *Nano Lett.* **2010**, *10*, 4475–4482.

(31) Dalacu, D.; Kam, A.; Austing, D. G.; Wu, X.; Lapointe, J.; Aers, G. C.; Poole, P. J. Selective-area vapour–liquid–solid growth of InP nanowires. *Nanotechnology* **2009**, *20*, 395602.

(32) Gibson, S.; LaPierre, R. Model of patterned self-assisted nanowire growth. *Nanotechnology* **2014**, *25*, 415304.

(33) Wenaas, E. P. Equilibrium cosine law and scattering symmetry at the gas–surface interface. *J. Chem. Phys.* **1971**, *54*, 376–388.

(34) Comsa, G.; David, R. Dynamical parameters of desorbing molecules. *Surf. Sci. Rep.* **1985**, *5*, 145–198.

(35) Dubrovskii, V. G.; Cirlin, G. E.; Soshnikov, I. P.; Tonkikh, A. A.; Sibirev, N. V.; Samosenko, Y. B.; Ustinov, V. M. Diffusion-induced growth of GaAs nanowhiskers during molecular beam epitaxy: Theory and experiment. *Phys. Rev. B* **2005**, *71*, 205325.

(36) Harmand, J.-C.; Glas, F.; Patriarche, G. Growth kinetics of a single $InP_{1-x}As_x$ nanowire. *Phys. Rev. B* **2010**, *81*, 235436.

(37) Scarpellini, D.; Fedorov, A.; Somaschini, C.; Frigeri, C.; Bollani, M.; Bietti, S.; Noetzel, R.; Sanguinetti, S. Ga crystallization dynamics during annealing of self-assisted GaAs nanowires. *Nanotechnology* **2017**, *28*, 045605.

(38) Bauer, B.; Rudolph, A.; Soda, M.; Fontcuberta i Morral, A.; Zweck, J.; Schuh, D.; Reiger, E. Position controlled self-catalysed growth of GaAs nanowires by molecular beam epitaxy. *Nanotechnology* **2010**, *21*, 435601.

(39) Krogstrup, P.; Jorgensen, H. I.; Johnson, E.; Madsen, M. H.; Sørensen, C. B.; Fontcuberta i Morral, A.; Aagesen, M.; Nygård, J.; Glas, F. Advances in the theory of III–V nanowire growth dynamics. *J. Phys. D: Appl. Phys.* **2013**, *46*, 313001.

(40) Glas, F.; Harmand, J.-C. Calculation of the temperature profile in nanowhiskers growing on a hot substrate. *Phys. Rev. B* **2006**, *73*, 155320.

(41) Wilson, D.; Sokolovskii, A.; LaPierre, R.; Panciera, F.; Glas, F.; Dubrovskii, V. G. Modeling the dynamics of interface morphology and crystal phase change in self-catalyzed GaAs nanowires. *Nanotechnology* **2020**,

(42) Plissard, S.; Dick, K. A.; Larrieu, G.; Godey, S.; Addad, A.; Wallart, X.; Caroff, P. Gold-free growth of GaAs nanowires on silicon: arrays and polytypism. *Nanotechnology* **2010**, *21*, 385602.

(43) Ambrosini, S.; Fanetti, M.; Grillo, V.; Franciosi, A.; Rubini, S. Vapor-liquid-solid and vapor-solid growth of self-catalyzed GaAs nanowires. *AIP Adv.* **2011**, *1*, 042142.

(44) Dubrovskii, V. G.; Sibirev, N. V.; Cirlin, G. E.; Harmand, J. C.; Ustinov, V. M. Theoretical analysis of the vapor-liquid-solid mechanism of nanowire growth during molecular beam epitaxy. *Phys. Rev. E* **2006**, *73*, 021603.

(45) Leshchenko, E. D.; Kuyanov, P.; LaPierre, R. R.; Dubrovskii, V. G. Tuning the morphology of self-assisted GaP nanowires. *Nanotechnology* **2018**, *29*, 225603.

(46) Priante, G.; Patriarche, G.; Oehler, F.; Glas, F.; Harmand, J.-C. Abrupt GaP/GaAs interfaces in self-catalyzed nanowires. *Nano Lett.* **2015**, *15*, 6036–6041.

(47) Spirkoska, D.; Arbiol, J.; Gustafsson, A.; Conesa-Boj, S.; Glas, F.; Zardo, I.; Heigoldt, M.; Gass, M. H.; Bleloch, A. L.; Estrade, S. et al. Structural and optical properties of high quality zinc-blende/wurtzite GaAs nanowire heterostructures. *Phys. Rev. B* **2009**, *80*, 245325.

(48) Dick, K. A.; Thelander, C.; Samuelson, L.; Caroff, P. Crystal phase engineering in single InAs nanowires. *Nano Lett.* **2010**, *10*, 3494–3499.

(49) Akopian, N.; Patriarche, G.; Liu, L.; Harmand, J.-C.; Zwiller, V. Crystal phase quantum dots. *Nano Lett.* **2010**, *10*, 1198–1201.